International Journal of Science and Research (IJSR)
ISSN (Online): 2319-7064
Index Copernicus Value (2013): 6.14 | Impact Factor (2013): 4.438

Enhancement of LVRT Capability of DFIG Wind Turbine by Using Advanced Control Strategy

PR. Manojprabu[1], V. Sudhagar[2]

[1]Student, Valliammai Engineering College, Chennai, Tamil Nadu, India,

[2]Assistant Professor, Valliammai Engineering College, Chennai, Tamil Nadu, India

Abstract: ***In this paper, doubly fed induction generator (DFIG) based wind turbine (WT) low voltage ride through (LVRT) capability is enhanced by using advanced control strategy for the rotor side converter (RSC) and grid side converter (GSC) to meet grid code requirements. The conventional crowbar with constant resistance method is used to protect and improve the LVRT. However, its response varies accordingly to the voltage dip level. In addition conventional method may be over or under estimate fault in certain condition which results in damage to the converters and DFIG. The proposed advanced control strategy introduces the instantaneous DC link current of the RSC as compensating term on GSC control scheme to smooth the DC link voltage fluctuations during the grid at the point of common coupling (PCC). By using pitch control, the wind energy is captured as rotor inertia during faults which significantly reduce the oscillations in the stator and rotor currents and the DC bus voltage during fault, the remaining energy is available to the grid after fault clearance and also it ensures smooth release of the excessive inertia energy into the grid. A time domain model for the 1.5 MW DFIG test system with the decoupled dq controller is implemented using MATLAB/SIMULINK and its effectiveness has been demonstrated through various simulation cases. The proposed control strategy results compared with conventional crowbar method shows not only the enhancement of LVRT capability of DFIG, but also helps maintaining continuous active and reactive power control during the grid fault.***

Keywords: Doubly fed induction generator (DFIG), wind turbine, low voltage ride through (LVRT), power system fault, MATLAB/Simulink.

1. Introduction

A doubly-fed induction generator (DFIG) is an adjustable-speed induction machine widely utilized in the modern wind power industry. The reasons for using variable speed wind turbines are fourfold: a higher energy yield, a reduction of mechanical loads and a simpler pitch control, an extensive controllability of both active and reactive powers, and less fluctuation in output power[1]. Increased penetration of wind generation in power grids is evident and is supported by being clean, renewable and having minimal running cost requirements.

On the other hand, the power grid holds some requirements for large-scale wind power to ensure its stability and to minimize the negative effects on the reliability of power grids, different countries have defined different low voltage ride through (LVRT) requirements for wind turbines (WT) in their grid codes[2]. To ensure the above requirement, the power grid requires the DFIG based wind turbine power system being connected to the power grid for a while in the lower voltage condition during the grid fault, which means that DFIG system should have fault ride through (FRT) capability for low voltage faults on the grid(LVRT) to prevent tripping of DFIG from the grid to assure reliability and without any damage to the DFIG system. In order to fulfill these LVRT requirements, the standard of LVRT requirement also included in grid code of different countries. The LVRT standard for American grid code is established as shown in Figure 1

Different approaches have been proposed to improve the wind turbine LVRT capability[3], [2], [4], [5]. Among the available control strategies, the crowbar protection is the mostly used. During the faults, the rotor side converter will be blocked, and the crowbar circuit is installed across the rotor terminals, will be triggered to damp the over-current in the rotor circuit. Consequently, the generator operates as a

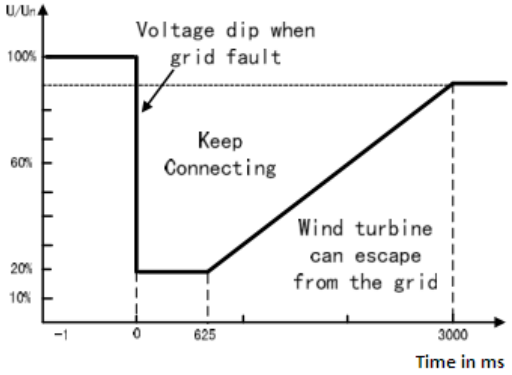

Figure 1: LVRT Standard of Grid code**.**

conventional induction machine, which absorbs reactive power from the faulted grid. The chopper circuit, with a resistor across the DC bus, is usually used along with the crowbar to smooth the DC-link voltage by dissipating the excessive power over the DC bus[3], [4], [6].

Based on the conventional crowbar protection, some improved crowbar solutions have been proposed to enhance the LVRT performance of the DFIG WT. Although the crowbar circuits are able to protect the machine and the converter during the faults, the controllability of the rotor converter with respect to the active and reactive power of the DFIG is temporarily lost. Moreover, the usage of crowbar and chopper actually installs extra hardware in the DFIG that can increase the costs and decrease the system reliability[6]. To overcome this problem, solution for reducing the inrush currents in the rotor as well as the DC-link over-voltage during the faults by means of designing adaptive controllers

for the rotor and grid side converters is proposed in [4],[3]. However, some of these algorithms are too complicated to implement in industrial applications and depend strongly on the proper design of the control parameters or the estimation of certain parameters, which may have adverse effects on its robustness[6].

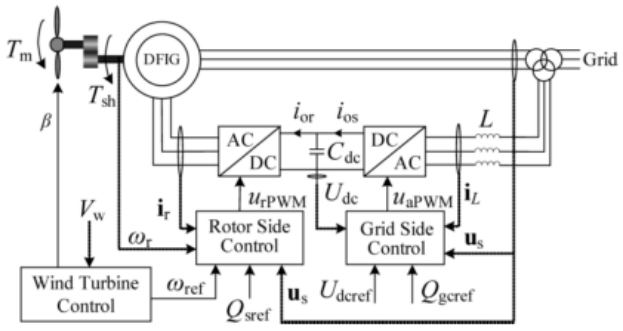

Figure 2: DFIG WT control and power flow scheme.

This paper presents the advanced control strategy for grid and rotor side converter of DFIG based WT to enhance the LVRT capability, without need of any additional circuits like crowbar and DC Chopper for protection. This is achieved by proper control on the rotor control scheme to increase generator rotor speed during a grid voltage dip at PCC. In conventional crowbar method the unbalanced energy during fault is dissipated in crowbar resistor whereas this unbalanced energy is converted to kinetic energy in proposed control strategy after clearance of fault. On other hand in grid side control scheme, a compensating term which reflects the variation on instantaneous DC- link current of the rotor side converter is added during fault to smooth the fluctuations of the DC-link voltage. The time domain model of a 1.5 MW DFIG test case system for simulation studies is simulated using MATLAB/Simulink.

The paper is organised as follows: Section 2 presents the model of the DFIG. Section 3 explains the proposed advanced control scheme for low voltage ride through (LVRT). Section 4 discusses the simulation results and finally conclusions are drawn in Section 5.

2. Modeling of the DFIG

The simple layout of DFIG WT control and power flow scheme is shown in figure 2. The DFIG WT system, including the wind turbine, the drive train, the induction generator, the back-to-back PWM converters, and the control system, is connected to the grid through a transformer[6]. In Sections 2.1–2.3, a detailed dynamic model of the DFIG WT will be presented.

2.1 Generator

The voltage equations of the stator and rotor circuits of the induction generator can be given in a reference frame rotating at the synchronous speed [1],[6].

$$u_{ds} = R_s i_{ds} - \omega_s \psi_{qs} + \frac{1}{\omega_b}\frac{d\psi_{ds}}{dt} \quad (1)$$

$$u_{qs} = R_s i_{qs} + \omega_s \psi_{ds} + \frac{1}{\omega_b}\frac{d\psi_{qs}}{dt} \quad (2)$$

$$u_{dr} = R_r i_{dr} - (\omega_s - \omega_r)\psi_{qr} + \frac{1}{\omega_b}\frac{d\psi_{dr}}{dt} \quad (3)$$

$$u_{qr} = R_r i_{qr} + (\omega_s - \omega_r)\psi_{dr} + \frac{1}{\omega_b}\frac{d\psi_{qr}}{dt} \quad (4)$$

where $\overrightarrow{i_s} = i_{ds} + j i_{qs}$ and $\overrightarrow{i_r} = i_{dr} + j i_{qr}$ are the stator and rotor current vectors, respectively; $\overrightarrow{u_s} = u_{ds} + j u_{qs}$ and $\overrightarrow{u_r} = u_{dr} + j u_{qr}$ are the stator and rotor voltage vectors, respectively; $\overrightarrow{\Psi_s} = \Psi_{ds} + j\Psi_{qs}$ and $\overrightarrow{\Psi_r} = \Psi_{dr} + j\Psi_{qr}$ are the stator and rotor flux vectors, respectively; $\omega_b, \omega_s,$ and ω_r are the base, stator, and rotor angular frequencies, respectively. The system model is written in the p.u. system with the time t, in seconds.

2.2 Drive Train

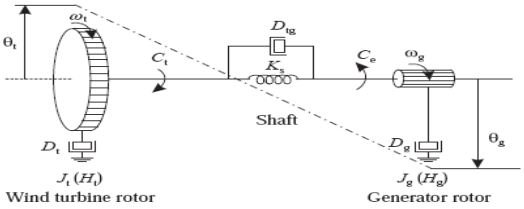

Figure 3: Two-mass model of a Drive train

The two-mass model of the drive train is important due to the wind turbine shaft is relatively softer than the typical steam turbine shaft in conventional power plants. The Figure 3 shows the two mass model of drive train. The equations which represent the two-mass model of the drive train are expressed as

$$\frac{d\omega_g}{dt} = \frac{1}{2H_g}\left(-T_e + K_{sh}(\theta_t - \theta_g) + D_{tg}(\omega_t - \omega_g)\right) \quad (5)$$

$$\frac{d\theta_t}{dt} = \omega_b(\omega_t - \omega_r) \quad (6)$$

$$\frac{d\omega_t}{dt} = \frac{1}{2H_t}\left(T_m - K_{sh}(\theta_t - \theta_g) - D_{sh}(\omega_t - \omega_g)\right) \quad (7)$$

where ω_t is the wind turbine speed. H_g and H_t [SI unit (s)] are the generator and turbine inertia constants, respectively. D_{sh} is the mutual damping, caused by differences in speeds of the rotor and the turbine shaft; and K_{sh} is the shaft stiffness. θ_t is the shaft twist angle, which is in radian (rad.). The electromagnetic torque T_e , the shaft torque T_{sh} , and the mechanical torque T_m , which is the torque input of the wind turbine, are

$$T_e = L_m(i_{qs} i_{dr} - i_{ds} i_{qr}) \quad (8)$$

$$T_{sh} = K_{sh}\theta_t + D_{sh}\omega_b(\omega_t - \omega_r) \quad (9)$$

$$T_m = \frac{0.5\rho\pi R^2 C_p(\lambda\ ,\ \beta)V_w^3}{\omega_t} \quad (10)$$

where ρ is the air density,R is the turbine radius, β is the pitch angle, V_w is the wind speed, C_p is the power coefficient, and

$$C_p = 0.22\left(\frac{116}{\lambda_i} - 0.4\beta - 5\right)e^{-12.5/\lambda_i} \quad (11)$$

$$\lambda_i = \frac{1}{\frac{1}{(\lambda + 0.08\beta)} - \frac{0.035}{(\beta^3 + 1)}} \quad (12)$$

where $\lambda = \omega_t R/V_w$ is the blade tip speed ratio, $C_p(\lambda, \beta)$ has a maximum value C_p^{max} for the optimal tip speed ratio λ_{opt} and optimized pitch angle β_{opt} .

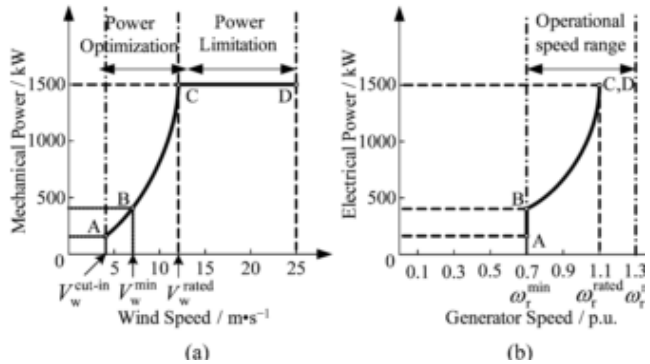

Figure 4: Two static curves used in the design of the DFIG WT. (a) Mechanical power versus wind speed. (b) Electrical power versus generator speed.

The wind turbine control is achieved by driving the generator/turbine speed along the optimum power-speed characteristic curve, illustrated in Figure. 4, which corresponds to the maximum energy capture from the wind. In this curve, when the wind speed is larger than the cut-in wind speed and less than the lower limit (zone A–B), the generator rotor speed reference for the rotor side controller is set as the minimal value ω_r^{min}, $\omega_r^{min} = 0.7\ p.u$ to ensure the generator slip smaller than 0.3. When the wind speed is between the lower limit and the rated value (zone B–C), the DFIG is operated in the variable speed mode, while λ is tuned to λ_{opt} over different wind speeds by adapting the generator speed to ω_{ref}, which can be obtained by substituting $\lambda = \omega_t R/V_w$ into (10),

$$\omega_{ref} = \sqrt{\frac{T_m}{K_{opt}}} \tag{13}$$

where $K_{opt} = \rho\pi R^5 C_p^{max}/2\lambda_{opt}^3$ is the optimal constant of wind turbine. Therefore, C_p can be maintained at C_p^{max} and the maximal power is achieved by tracking in (13). When the wind speed is higher than the rated value (zone C-D), is set as the rated value of the generator speed, the over rated turbine power production will be restrained by the pitch control, which can therefore limit the over-speed of the generator.

2.3 Pitch Control

The pitch angle of the blade is controlled to optimize the power extraction of the WT as well as to prevent over rated power production in high wind. The pitch servo is modeled as

$$\frac{d\beta}{dt} = \frac{1}{T_\beta}(\beta_{ref} - \beta) \tag{14}$$

The pitch control scheme is shown in Figure 3 was proposed in [6]. When the generator speed exceeds ω_r^{rated}, the pitch control is active and the pitch angle is tuned so that the turbine power can be restricted to its rated value.

The blades are rotated by using electrical or hydraulic devices (servos) and allow the pitch angle β to be varied between 0^0 and 25^0 (up to 30^0). When the wind speed drops below the cut-in speed, the power can be cancelled by turning the blades at $\beta = 90^0$.

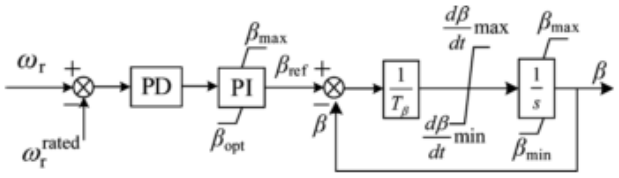

Figure 5: Schematic diagram of the pitch control.

.

3. Proposed Low Voltage Ride Through Strategy

3.1 Overview of the Proposed Control Strategy

When the power grid is subject to, e.g., a short-circuit fault, the bus voltage at the PCC drops, and therefore introducing undesirable transients in the stator and rotor currents. The low voltage also prevents the full transmission of generated active power from the WT, leading to significantly increased fluctuations of the currents and voltages in the DFIG system. In order to protect the power electronics devices that are sensitive to over-currents and over-voltages, the purpose of introducing the LVRT strategy is to ensure the DFIG can stay connected to the faulted grid by effectively limiting the stator and rotor circuit currents as well as the DC-link voltage.

The conventional crowbar control realizes the LVRT protection by blocking the rotor side converter circuit and introducing additional rotor winding resistances that actually dissipate the produced energy. In contrast, the proposed control strategy can transform the additional output power into the WT kinetic energy by temporarily increasing the generator rotor speed during the grid faults, thus effectively limiting the oscillations in the currents. The proposed control strategy makes full use of existing resources within the DFIG WT system to realize the LVRT without the need of additional components like the crowbar.

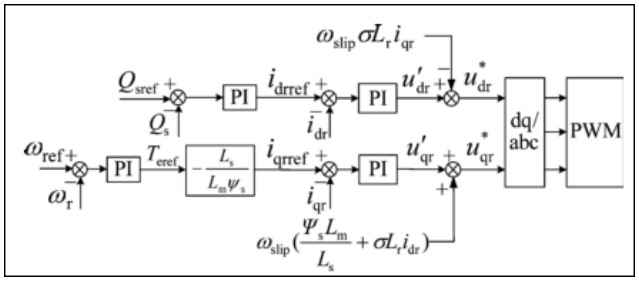

Figure 6: Control scheme of the rotor side converter in normal operation.

It can effectively protect the power electronics devices against current and voltage fluctuations during grid faults to ensure the LVRT of the DFIG. Several advantages can be achieved by using the new control strategy. From the energy perspective, the new control strategy can absorb the additional output power during the faults that will be otherwise dissipated in the crowbar based control. Notably, the increased kinetic energy of the WT can be released into the grid slowly after the fault clearance. From the control perspective, the new control strategy can ensure the back-to-back converters well connected to the DFIG as well as the grid without loss of the controllability during the faults. This potentially can enable both active and reactive supports to

the faulted grids from WT which is difficult for the crowbar based control. The detailed control scheme will be illustrated in Sections 3.2 and 3.3, and the simulation validation will be given in Section 4.

3.2 Control of Rotor Side Converter (RSC)

In normal operation, the control scheme of the RSC is illustrated in Figure 6. In order to decouple the electromagnetic torque and the rotor excitation current, the induction generator is controlled in the stator-flux oriented reference frame, which is a synchronously rotating reference frame, with its axis oriented along the stator-flux vector position (in this paper, the stator-flux vector is calculated using) [1]. The typical proportional-integral (PI) controllers are used for regulation in the rotor speed and reactive power (outer) control loops as well as the rotor cur- rent (inner) control loops[6]. The values of ω_{ref} , generated by the wind turbine control level, at different operation conditions have been defined in Section 2. When a short-term low-voltage fault occurs, the incoming power from the wind and the power flowing into the grid are imbalanced instantaneously, resulting in the transient excessive currents in the rotor and

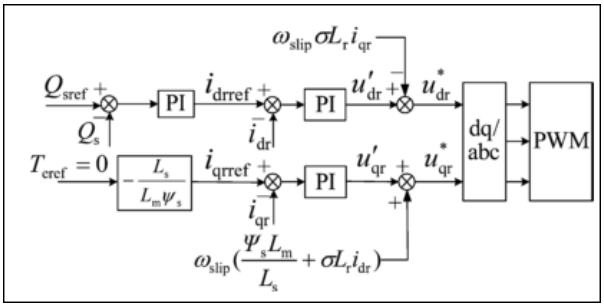

Figure 7: Control scheme of the rotor side converter during a grid fault.

stator circuits. When at least one of the monitored parameters, including stator current and DC-link voltage exceeds its respective protection setting due to the grid fault, the proposed LVRT control strategy will be triggered. With this control strategy, the rotor side controller will increase the generator rotor speed by reducing the generator torque to zero during the fault, in order to absorb and convert the incoming energy from the wind into the kinetic energy in the WT inertia. The increased kinetic energy can be transformed and released into the grid after the fault clearance.

The control scheme of the RSC against grid faults is illustrated in Figure 7. The parameters of the PI controllers was given in [6]. The new control strategy will not cause excessive mechanical stress to the WT system. This analysis will be verified by the simulation results in Section 4.

3.3 Control of Grid Side Converter (GSC)

Figure 8 shows the control scheme of the GSC in normal operation, where u_a and i_L are the grid-side converter voltage vector and the grid-side inductor current vector, respectively. In order to obtain the independent control of active and reactive power flowing between the grid and the GSC, the converter control operates in the grid-voltage oriented reference frame, which is a synchronously rotating reference frame, with its axis oriented along the grid-voltage vector position. Similarly, the typical PI controllers are used [6].

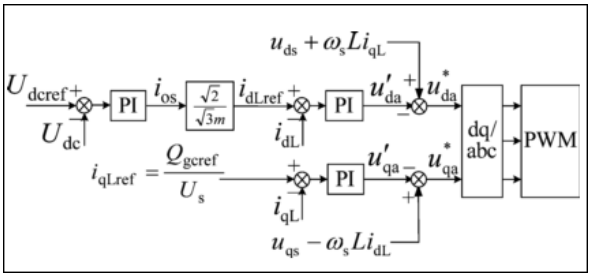

Figure 8: Control scheme of the grid side converter in normal operation.

The equation which describes the dynamic behavior of the DC-link capacitor can be expressed as

$$C_{dc}\frac{dU_{dc}}{dt} - i_{os} - i_{or} = 0 \quad (15)$$

where i_{os} and i_{or} are the DC-link currents of the grid and rotor side converters, respectively. Neglecting the losses in the inductor resistances and power electronics converters, we have

$$i_{os} = \frac{\sqrt{3}}{\sqrt{2}} i_{dL} \quad (16)$$

$$i_{or} = \frac{P_r}{U_{dc}} \quad (17)$$

where P_r is the magnitude of the active power of the generator rotor. In normal operation, when the power flowing through the grid and rotor side converters is balanced, i_{os} is equal to i_{or} , so the DC-link voltage is constant. During grid voltage dip, the fluctuation of the DC-link voltage is reduced by the item (P_r/U_{dc}) reflecting the instantaneous variation of the output power of the rotor side controller is directly set as the reference of the during the grid fault. However, the stator voltage may reduce to zero during the grid fault. This will introduce an extremely high transient value of i_{dL} .

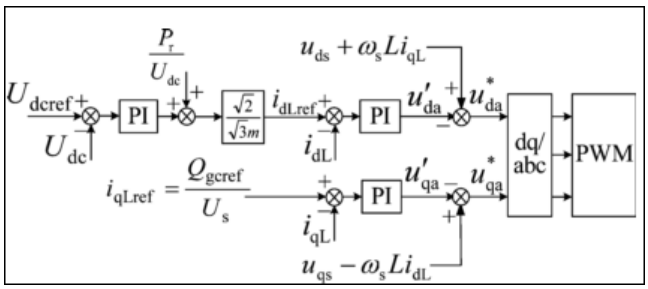

Figure 9: Control scheme of the grid side converter during a grid fault.

In this paper, when the rotor current, stator current, DC-link voltage, or grid voltage exceeds its respective relay setting due to the grid voltage dip, the term (P_r/U_{dc}) describing is represented as a disturbance to compensate the instantaneous rotor power in the control scheme. In such away, the can be regulated smoothly during a grid fault. The detailed control scheme of the GSC during the grid fault is shown in Figure. 9.

4. Simulation and Results

The DFIG WT under study is connected to the grid transmission level via a radial link as shown in Figure 10. In order to evaluate the proposed control strategy, the complete DFIG WT system model has been developed and simulated in MATLAB/Simulink environment as shown in Figure11. The components of the simulation model are built with SimPower Systems block in MATLAB/Simulink library. The parameters of the studied DFIG WT are listed in the Appendix.

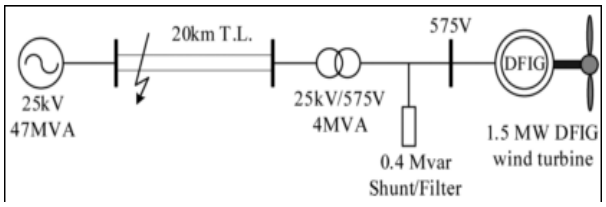

Figure 10: Single line diagram for the studied system.

Two different control strategies of LVRT on the performance of the studied DFIG WT during different symmetrical three-phase short-circuit faults are investigated to study their effects, including

Strategy A: The conventional protective system equipped with crowbar and DC-link chopper.

Strategy B: The proposed control strategy of RSC and GSC.

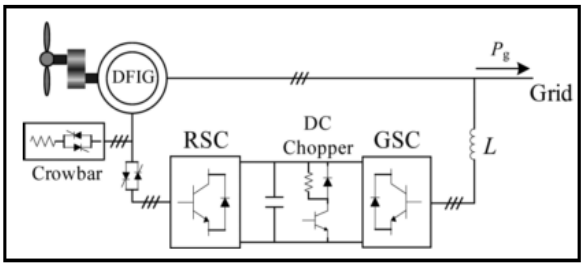

Figure 111: DFIG WT with the crowbar and DC chopper protection circuits.

The DFIG WT with the crowbar and DC chopper protection circuits of the strategy A is shown in Figure 11 was simulation in MATLAB/Simulink as shown in Figure 12. The crowbar circuit includes the controllable switches and resistors. The crowbar resistors is chosen as $40R_r$. The DC chopper resistor is selected as 0.5 p.u. The protection threshold of rotor and stator currents are both set to 2 p.u. The detailed scheme of the crowbar protection is described in [4].

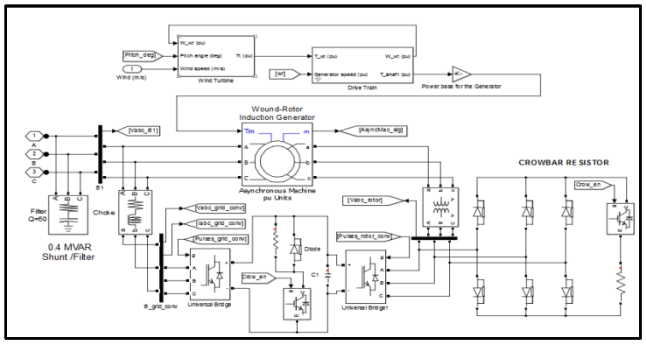

Figure 122: MATLAB/SIMULINK Diagram for DFIG WT with crowbar and DC Chopper Protection Circuit

4.1 Simulation of Power converter

The Figure 13 shows the MATLAB/SIMULINK Model of Rotor side Converter with compensating FRT Signal Block whose output is controlled by FRT_en Signal to select Crowbar or LVRT Control Techniques. The pulse signal to Rotor side Converter is made zero (Disabling RSC triggering) by Crow_en signal during fault in Crowbar Control Strategies.

The Figure14 shows the MATLAB/Simulink Model of Grid side controller with compensating Fault ride through block whose output is enabled by FRT_en during implemen-ting LVRT Control Strategy, otherwise output signal is disabled when implementing crowbar Control Strategy.

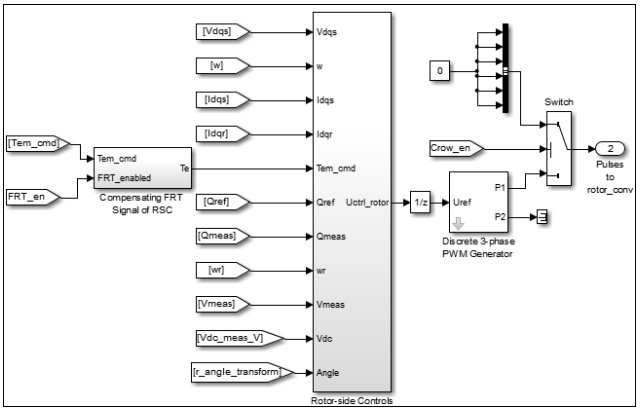

Figure 133: MATLAB/SIMULINK Model of Rotor Side Converter.

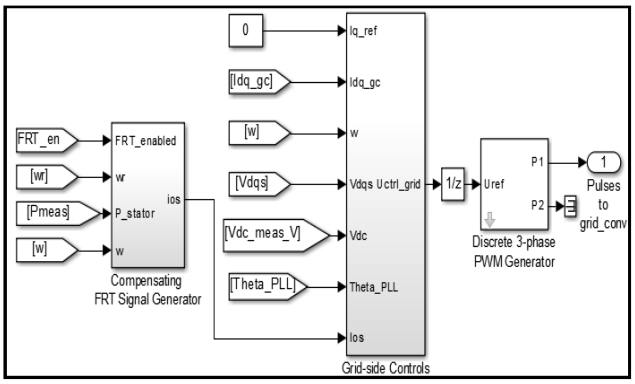

Figure 144: MATLAB/SIMULINK Model of Grid Side Controller

4.2 Simulation Results

The result comparison are made for conventional Crowbar Resistance and LVRT Implementation on Rotor and Grid Side converter of the DFIG and result are generated for the following cases.

Case 1: Conventional Crowbar Resistor with R_{cb}=40R_r with Low and High Wind Speed with Symmetrical fault duration of 625 ms.

Case 2: LVRT Control Strategy with Low and High Wind Speed with Symmetrical fault duration of 150ms and 625ms.

4.2.1. Conventional Crowbar Resistor Results

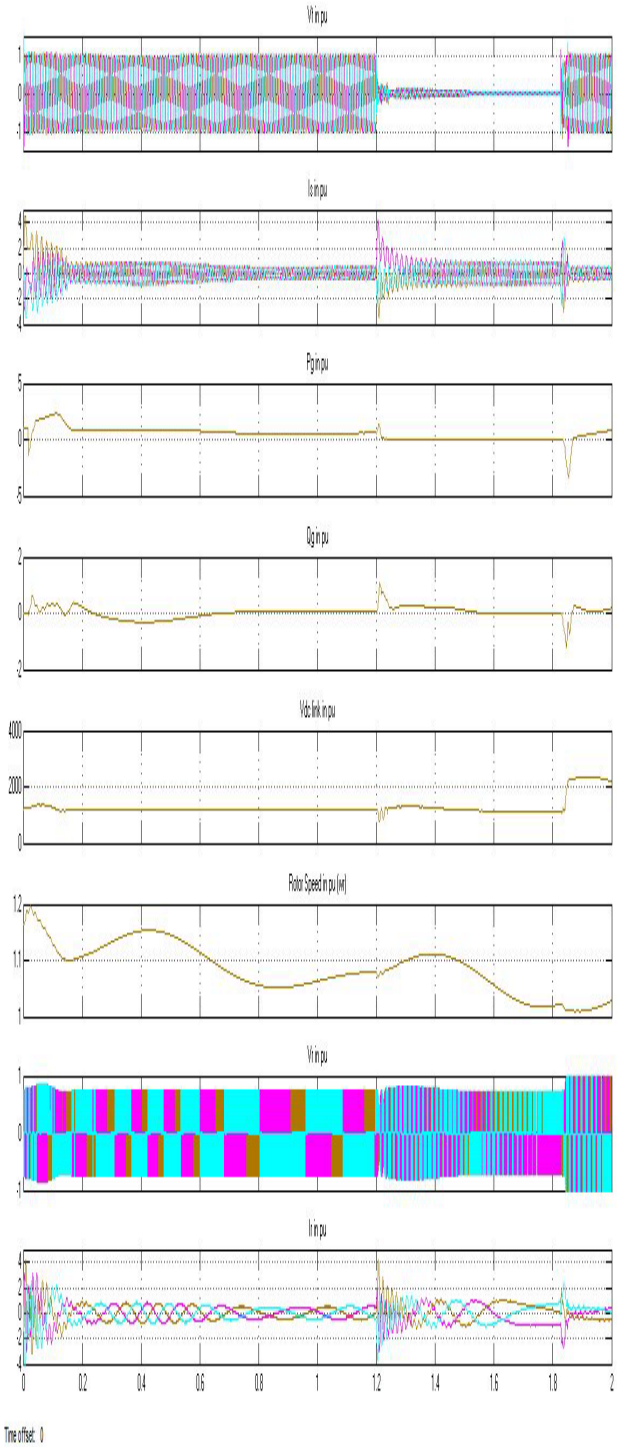

Figure 155: DFIG WT at wind speed of 8 m/s with the crowbar control strategies fault duration of 625ms in PCC.

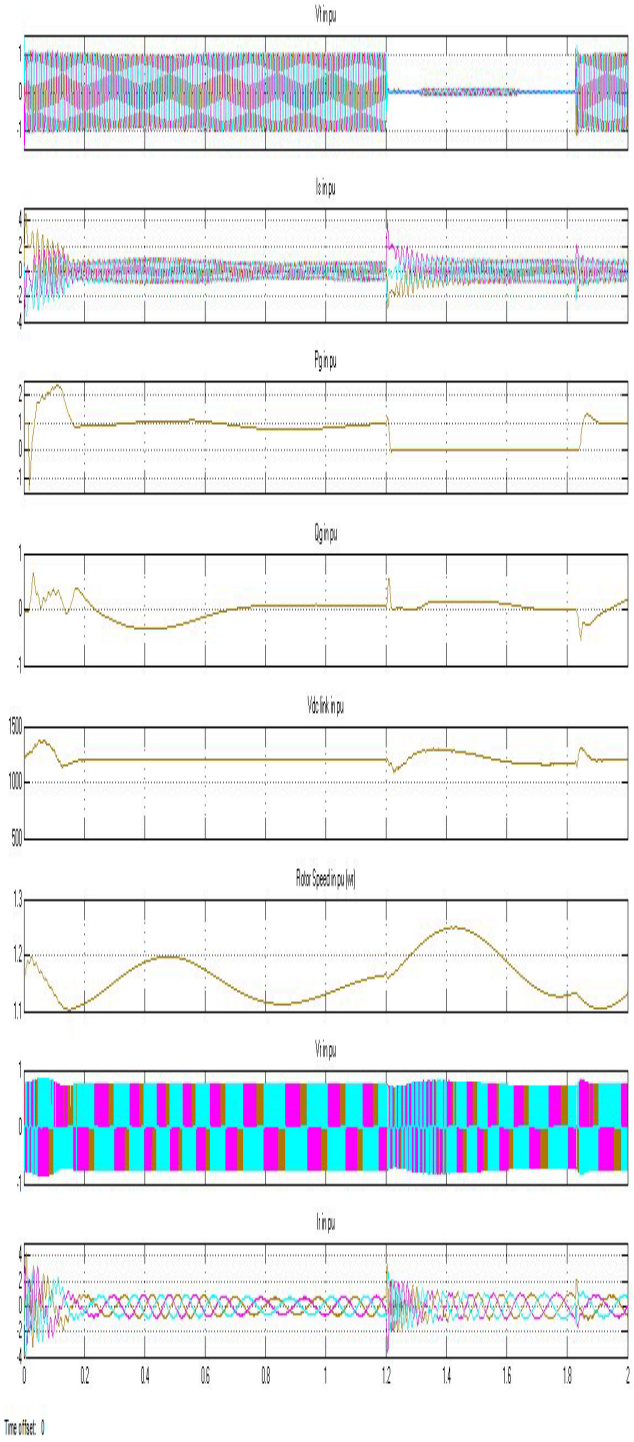

Figure 166: DFIG WT at wind speed of 14 m/s with the crowbar control strategies fault duration of 625ms in PCC.

The Figure 15 shows Simulated Transient response of DFIG WT Crowbar Strategies at low Wind Speed of 8m/s with symmetrical fault duration of 625ms at PCC between Time Period 1.2 to1.825 sec, I_r in pu does not exceed 2 p.u during fault and rotor de-accelerates after fault cleared due to the power losses in crowbar resistance during fault, so DFIG can delivers less Active Output to grid and also draws reactive power from the grid. This may cause Grid unstable, if Grid has no or less Reactive support may lead to tripping of DFIG WT from Grid.

The Figure 16 shows the transient response of DFIG WT Crowbar Strategies during the high wind speed 14m/s with Symmetrical Fault Duration of 625ms at PCC between time period of 1.2 to 1.825 sec, I_r in p.u does not exceed 2 p.u, After fault Cleared, Active Power rate of rise is high and reactive power drawn from the grid is less compared to previous condition shown in Figure 15.

4.2.2. LVRT Control Strategy Results

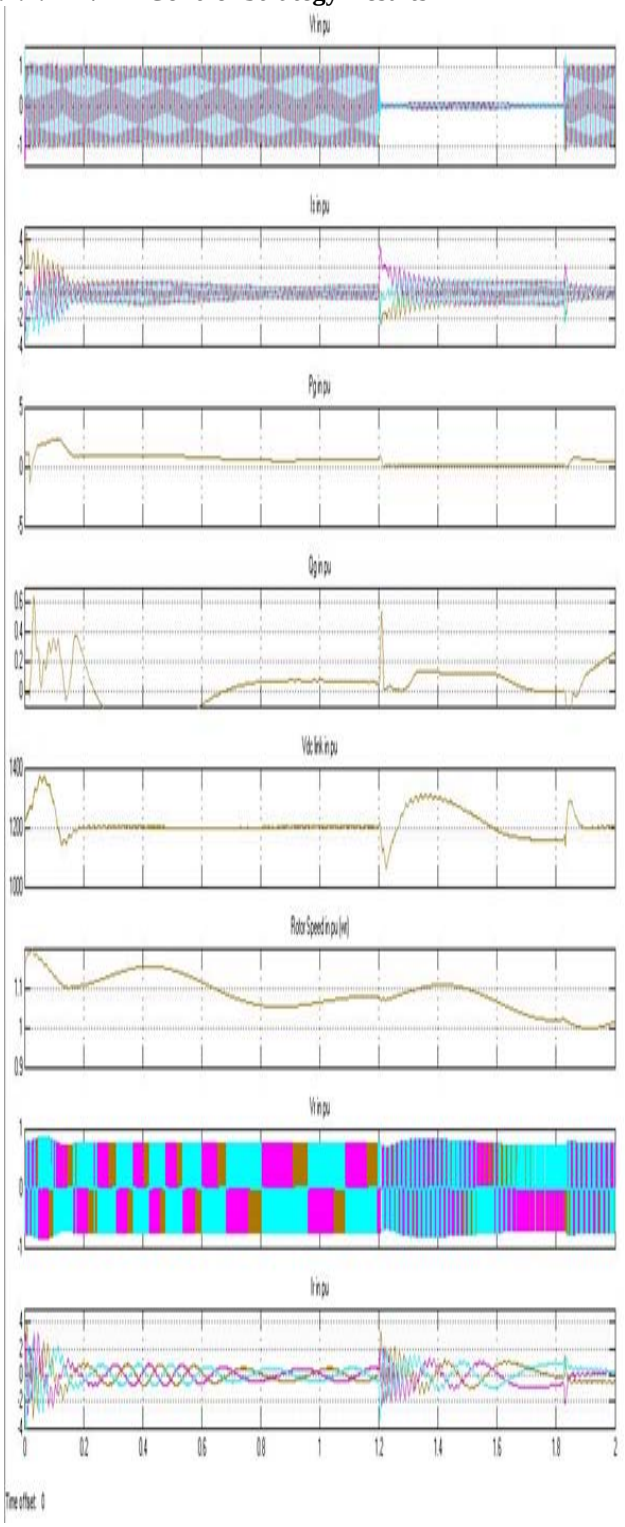

Figure 17: DFIG WT at wind speed of 8 m/s with the LVRT control strategies fault duration of 625ms in PCC.

The Figure 17 shows the transient responses of the studied DFIG WT LVRT Control Strategies at low Wind Speed of 8m/s with symmetrical fault duration of 625ms at PCC between Time Period 1.2 to1.825 sec, I_r in pu does not exceed 2 p.u during fault. After fault cleared, the reactive power is delivered to the grid.

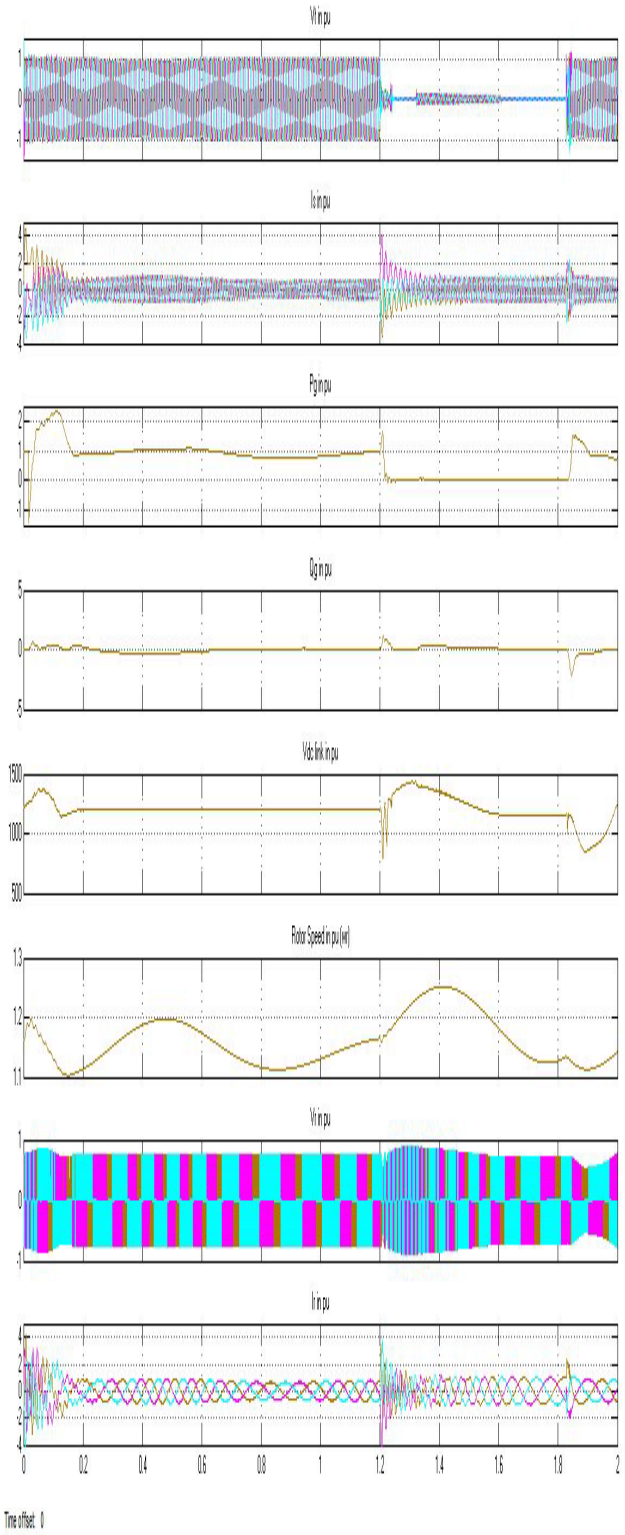

Figure 18: DFIG WT at wind speed of 14 m/s with the LVRT control strategies fault duration of 625ms in PCC.

The Figure 18 shows the transient responses of the studied DFIG WT LVRT Control Strategies at high Wind Speed of 14m/s with symmetrical fault duration of 625ms at PCC between Time Period 1.2 to1.825 sec, I_r in pu does not exceed 2 p.u, active and reactive power drawn is zero during fault. At Clearance of fault, the rate of rise active power delivered to grid is high and no reactive power is drawn from the grid.

5. Conclusion

During fault and under low wind speed, the acceleration of the generator rotor with the LVRT control strategy is faster than the conventional crowbar technique so the active acceleration can transform the additional energy into the grid at instant of fault clearing. In the proposed control strategy, grid side converter compensating component (P_r/U_{dc}) is introduced during fault which can reduce the overvoltage on the DC Bus. Similarly the compensating term in the rotor side converter will suppress the oscillation in the speed after clearance of fault and rotor speed reduces back to the reference value.

During Over speed and faults condition, RSC effectively restrained by pitch control and prevents the conversion of electric energy to kinetic energy. By comparing the DC-lick Voltage on high wind speed, the fluctuation is very high with conventional Crowbar techniques compared to LVRT Technique. Due to the addition of Fault Ride through Strategy on grid side converter, the fluctuation in DC-Link voltage has been reduced.

By comparing simulation result of Conventional Crowbar Control Technique with the Proposed LVRT System for 1.5MW DFIG Studied System shows that rotor current during fault lies within 1.5 p.u, the voltage across DC Link not exceeds 1.2 p.u, the rate of rise of active power delivered to grid after clearance of fault is high and also DFIG deliver reactive power to the grid after fault Cleared. The DFIG WT installed with the proposed control strategy gives a better transient behavior in event of short-term grid voltage dip. By using the new control strategy, little impact will be resulted to the WT mechanical construction and the occurrence of the crowbar interruption can also be minimized.

Appendix

The parameters of the studied DFIG WT are as follows:
Wind turbine: cut-in wind speed: 4 m/s; lower limit of the wind speed: $V_w^{min} = 7m/s$; rated wind speed: 12 m/s; inertia constant: $H_t = 3s$; damping coefficient: $D_{sh} = 0.01\ p.u$;shaft stiffness coefficient: $K_{sh} = 0.5\ p.u$; time constant of the pitch servo: $T_\beta = 0.25\ s$.
DFIG: rated power: 1.5MW; rated voltage: 575 V; rated current; 1505 A; rated rotor speed: $\omega_r^{rated} = 1.1\ p.u$(with the synchronous speed as the base value); inertia constant: $H_g = 0.5\ s$; friction coefficient: $B = 0.01\ p.u$; stator resistance: $R_s = 0.00706\ p.u$; rotor resistance: $R_r = 0.005\ p.u$; stator leakage inductance: $L_{ls} = 0.171\ p.u$; rotor leakage inductance: $L_{lr} = 0.156\ p.u$; mutual inductance: $L_m = 3.5\ p.u$.
Converters: resistance of grid side inductor:$R_L = 0.003\ p.u$; inductance of grid side inductor: $= 0.3\ p.u$; DC-link capacitor: $C_{dc} = 0.06F$.

References

[1] S. Li, R. Challoo, and M. J. Nemmers, "Comparative study of DFIG power control using stator-voltage and stator-flux oriented frames," in *2009 IEEE Power & Energy Society General Meeting*, 2009, pp. 1–8.
[2] A. H. Kasem, E. F. El-Saadany, H. H. El-Tamaly, and M. A. A. Wahab, "An improved fault ride-through strategy for doubly fed induction generator-based wind turbines," *IET Renew. Power Gener.*, vol. 2, no. 4, pp. 201–214, Dec. 2008.
[3] D. Xie, Z. Xu, L. Yang, J. Ostergaard, Y. Xue, and K. P. Wong, "A Comprehensive LVRT Control Strategy for DFIG Wind Turbines With Enhanced Reactive Power Support," *IEEE Trans. Power Syst.*, vol. 28, no. 3, pp. 3302–3310, Aug. 2013.
[4] Zhang Jian, Xue Ancheng, Chen Jinmei, Bi Tianshu, Wang Ningbo, and Ma Yanhong, "An adaptive LVRT control for DFIG wind power system." pp. 6747–6751, 2012.
[5] S. Abulanwar and F. Iov, "Enhanced LVRT control strategy for DFIG-based WECS in weak grid," in *2013 International Conference on Renewable Energy Research and Applications (ICRERA)*, 2013, pp. 476–481.
[6] L. Yang, Z. Xu, J. Ostergaard, Z. Y. Dong, and K. P. Wong, "Advanced Control Strategy of DFIG Wind Turbines for Power System Fault Ride Through," *IEEE Trans. Power Syst.*, vol. 27, no. 2, pp. 713–722, May 2012.

Author Profile

PR.Manojprabu received his Bachelor's degree in Electrical and Electronics Engineering from Jeppiaar Engineering College, Chennai in 2013 and he is pursuing Master's degree in Power Systems Engineering in Valliammai Engineering College, Chennai. His area of interest is power system and wind energy conversion system.

V.Sudhagar obtained his BE degree in Electrical and Electronics Engineering in 2007 and obtained his Master's degree in Power Systems Engineering from College of Engineering, Guindy in 2010. His field of interest is power systems, power quality and renewable energy systems. He has teaching experience of 7 years. Currently, he is working as an Assistant Professor in Department of Electrical and Electronics Engineering at Valliammai Engineering College, SRM Nagar, Kattankulathur, Chennai.